

Vision Transformer Off-the-Shelf: A Surprising Baseline for Few-Shot Class-Agnostic Counting

Zhicheng Wang

zc_wang@hust.edu.cn

School of Artificial Intelligence and Automation
Huazhong University of Science and Technology PRC

Zhiguo Cao

zgcao@hust.edu.cn

School of Artificial Intelligence and Automation
Huazhong University of Science and Technology PRC

Liwen Xiao

lwxiao@hust.edu.cn

School of Artificial Intelligence and Automation
Huazhong University of Science and Technology PRC

Hao Lu

hlu@hust.edu.cn

School of Artificial Intelligence and Automation
Huazhong University of Science and Technology PRC

ABSTRACT

Class-agnostic counting (CAC) aims to count objects of interest from a query image given few exemplars. This task is typically addressed by extracting the features of query image and exemplars respectively with (un)shared feature extractors and by matching their feature similarity, leading to an extract-then-match paradigm. In this work, we show that CAC can be simplified in an extract-and-match manner, particularly using a pretrained and plain vision transformer (ViT) where feature extraction and similarity matching are executed simultaneously within the self-attention. We reveal the rationale of such simplification from a decoupled view of the self-attention and point out that the simplification is only made possible if the query and exemplar tokens are concatenated as input. The resulting model, termed CACViT, simplifies the CAC pipeline and unifies the feature spaces between the query image and exemplars. In addition, we find CACViT naturally encodes background information within self-attention, which helps reduce background disturbance. Further, to compensate the loss of the scale and the order-of-magnitude information due to resizing and normalization in ViT, we present two effective strategies for scale and magnitude embedding. Extensive experiments on the FSC147 and the CARPK datasets show that CACViT significantly outperforms state-of-the-art CAC approaches in both effectiveness (23.60% error reduction) and generalization, which suggests CACViT provides a concise and strong baseline for CAC. Code will be available.

CCS CONCEPTS

• **Computing methodologies** → **Computer vision**; • **Human-centered computing** → Visualization design and evaluation methods.

KEYWORDS

Class-agnostic counting, Transformer models, Self-attention

1 INTRODUCTION

Object counting aims to estimate the number of objects from a query image. Most prior object counting approaches target a specific domain, e.g., crowd [26, 32, 33], plant [20, 22], and car [23]. They often require numerous class-specific training data to learn a good model [28]. In contrast, Class-Agnostic Counting (CAC), whose goal is to estimate the counting the value of arbitrary categories

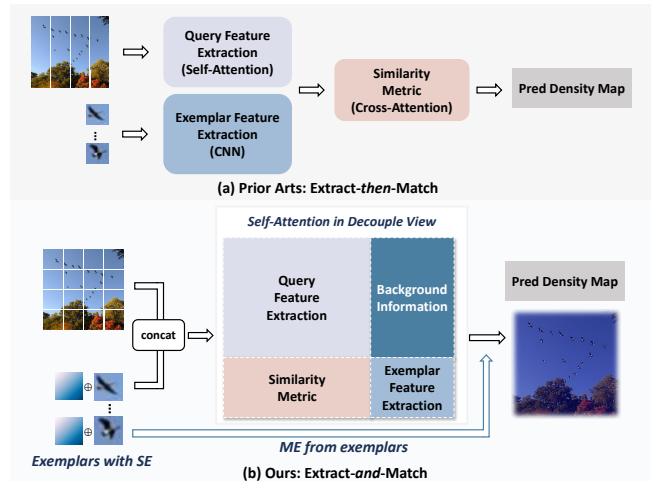


Figure 1: High-level ideas between prior arts and ours. (a) Previous ViT-based class-agnostic counting framework follows the extract-then-match paradigm with unshared feature extractors (e.g., a ViT and a CNN) for the query image and the exemplars and post-matching such as cross-attention after feature extraction; (b) Our ViT-based framework follows an extract-and-match paradigm using self-attention in a decoupled view, with additional aspect-ratio-aware scale embedding (SE) and the order-of-magnitude embedding (ME) for compensating the information loss of the scale in ViT.

given only few exemplars, has recently received much attention due to its potential to generalize to unseen scenes and reduced reliance on class-specific training data [16, 19, 24, 25].

Since CAC is first introduced by Lu *et al.* [19], this task is by default formulated as a template-matching-like problem, leading to an extract-then-match paradigm. Typical CAC approaches generally follow this paradigm [16, 24, 25]. For example, BMNet [25] uses a shared Convolution Neural Network (CNN) backbone to extract features of the query image and exemplars, and then applies a learnable bilinear similarity metric for matching. In this paper, our key finding is that CAC can be simplified and addressed in

an extract-*and*-match manner with only the self-attention mechanism [27].

Vision Transformer (ViT) [4], which adopts the self-attention mechanism, has significantly improved crowd counting recently [12, 14]. Being the first to adopt the ViT to CAC, CounTR [16], which also follows the extract-then-match paradigm, uses the ViT to extract features of the query image and a CNN to extract exemplar features, and then, performs feature matching with cross-attention. However, the heterogeneous feature extraction backbones can render inconsistency of feature spaces, thus requiring strong post-matching such as the six cross-attention layers used in CounTR to compensate the inconsistency.

In this work, we show that, by grouping the query and exemplar tokens in a concatenated form and feeding them to a plain ViT, the self-attention in ViT would naturally execute the feature extraction and the feature matching internally and simultaneously, without extra post-matching, producing a novel extract-*and*-match paradigm. This new paradigm naturally unifies the feature space and simplifies the model design. In particular, we discuss why such simplification makes sense and how it works in self-attention from a decoupled view. This view enables us to see that self-attention not only extracts query and exemplar features and matches their similarity as in previous CAC models, but also encodes background information, as shown in Fig. 1. In particular, the attention from the query image to exemplars can be regarded as background information, which can be used to filter out background noise and to facilitate precise localization.

While we claim that the self-attention mechanism in ViT spontaneously suiting the CAC task, certain restrictions or functions such as resizing and softmax normalization within this architecture can result in the loss of scale information and the order of magnitude of counting values. First, the exemplars must be resized to fit the ViT input, which introduces size ambiguity during matching. Prior CNN-based models [25] attempt to compensate for the scale information with scale embedding for exemplars; however, they neglect the information of aspect ratios, which is crucial for classes with abnormal ratios. This is largely overlooked in the existing literature. Second, the softmax function used in self-attention can affect the relative distribution of objects in the query image and therefore weakens the awareness of the model to the number of objects. We address this by restoring the magnitude order in the normalized attention map. Both the proposed scale embedding and magnitude embedding are easy to implement. By infusing the scale and the magnitude information into the plain ViT architecture, we acquire a surprisingly simple yet highly effective ViT baseline for CAC. The resulting model, termed CACViT, fully leverages the self-attention mechanism in ViT while also being tuned to mitigate the defects of this architecture in this task.

Experiments on the public benchmark FSC147 [24] show that CACViT outperforms the previous best approaches by large margins, with relative error reductions of 19.04% and 23.60% on the validation and test sets, respectively, in terms of mean absolute error. Its cross-dataset generalization is also demonstrated on a car counting dataset CARPK [9]. We also provide extensive ablation studies to justify our propositions.

In a nutshell, our contributions are three-fold:

- A novel extract-*and*-match paradigm: we show that simultaneous feature extraction and matching can be made possible in CAC;
- CACViT: a simple and strong ViT-based baseline for CAC, which sets the new state of the art on the FSC-147 benchmark;
- We introduce two effective strategies to embed scale, aspect ratio, and order of magnitude information tailored to CACViT.

2 RELATED WORK

The task of CAC is composed of two main components: feature extraction and feature matching. We review each component in previous counting models.

Feature Extraction in Class-Specific Counting. Feature extraction is a fundamental problem. The investigation of feature extraction in counting first began with class-specific counting [1–3, 8, 10, 11, 17, 29]. In class-specific counting, most of the available works are designed to address the challenges posed by quantity variance between images and scale variance within an image. For instance, Ma *et al.* [21] propose a scale-aware probabilistic model to mitigate the perspective effects. Given that the transformer model [27] has been used in a wide range of machine-learning areas, some work [12–14] also uses the transformer as a feature extractor in counting, which can capture the global contextual information by built-in attention mechanism. For example, Lin *et al.* [14] propose a multifaceted attention network to improve transformer models in local spatial relation encoding, which can use the global contextual information to obtain the quantitative information for different images and use the local information to infer the scale variation.

Feature Extraction in Class-Agnostic Counting. For class-agnostic counting, the core of feature extraction not only includes quantity and scale variation as above but also requires unified matching space and the suppression for out-of-interest objects, *i.e.*, background suppression. To obtain a unified matching space, most previous work [24, 25, 31] uses the shared CNN-based feature extractors for query images and exemplars. In this way, a strong feature matcher must be used as well. CounTR [16], which first introduces the ViT for feature extraction in CAC, but uses different feature extractors for the query images (a ViT) and exemplars (a CNN). Hence, multiple layers of cross-attention are used for matching. In addition, few work focuses on suppressing the background noise in CAC. In our work, by regarding exemplars as extra tokens of the query image, we use a shared ViT for feature extraction and feature matching and also take background information embedded in self-attention into account.

Feature Matching in Class-Agnostic Counting. Compared with feature extraction, matching strategies in CAC have garnered more attention. The key points of the matching include the following two: 1) robustness to appearance variance, *e.g.*, shape, size, and color and 2) ability to characterize quantity levels. In the early attempt, naive inner product [24, 30] is used for matching, which is not robust to the appearance variance of objects to be counted. Shi

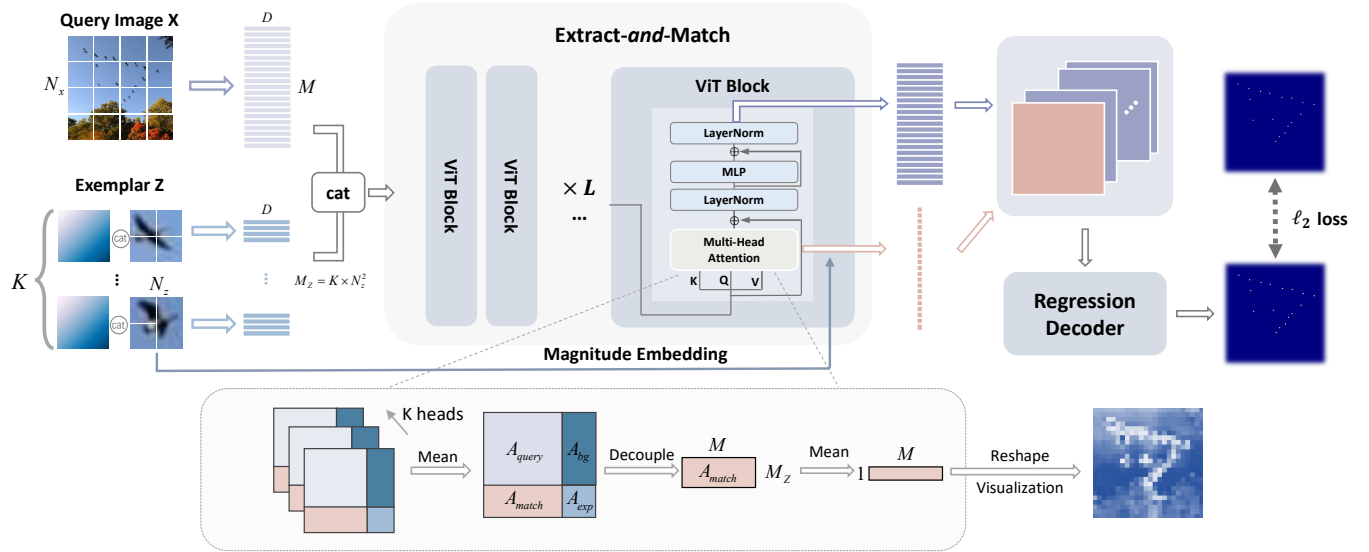


Figure 2: The framework of CAC Vision Transformer (CACViT). A query image and exemplars with scale embedding are split into patches to form tokens. Then the flattened tokens are concatenated and fed into the transformer encoder. Afterwards, the output feature of query image and similarity metric from attention map are concatenated for regression. Finally, a regression decoder predicts the density map. ℓ_2 loss are used to supervised the training process.

et al. [25] developed a bilinear matching network (BMNet) that expands the fixed inner product to a learnable bilinear similarity metric, which improves the robustness compared with the inner product. The recent ViT-based model CounTR [16] uses cross-attention for matching, which seems a natural choice for a transformer-based solution at a first glance. However, we show that, in our plain ViT model CACViT, we can perform feature matching at the same time of extracting features by self-attention. This largely simplifies the model design.

3 CLASS-AGNOSTIC COUNTING VISION TRANSFORMER

In this section, we first introduce the overview of our framework for CAC, named Class-Agnostic Counting Vision Transformer (CACViT). Then, we provide analysis for why the pure self-attention layers could serve as substitution for previous architectures. After the ViT-style model is established, we spot the problem of scale information loss when directly applying ViT, and provide customized solutions for scale compensation.

3.1 Overview of Approach

The pipeline of CACViT is presented in Figure 2. A query image \mathcal{X} and corresponding exemplars \mathcal{Z} , which are resized to a fixed exemplar size, are split into tokens. Then they are concatenated and processed by self-attention layers. Afterward, the output feature of the query image and the similarity map from the last attention map are concatenated to form the final density map. The ℓ_2 loss is adopted to supervise the density map.

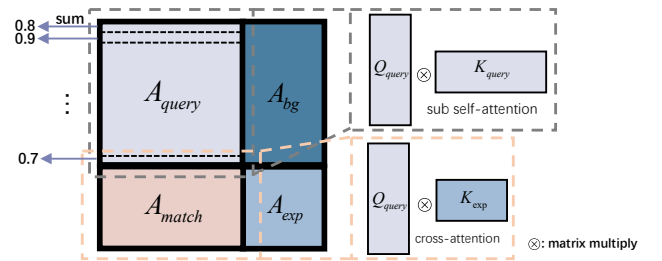


Figure 3: Decoupled view of self-attention in CACViT. The top-left A_{query} can be regarded as self-attention of the query image, whose sum of every row is less than 1 because of A_{bg} . The bottom-left A_{match} can be interpreted as cross-attention between query images and exemplars, despite being implemented in self-attention.

3.2 A Decoupled View of Self-Attention

We follow the standard formulation of self-attention in CACViT. Yet, in the presence of both query and exemplar tokens, we have a different interpretation of self-attention in CAC.

We first revisit self-attention in transformer. Given an input token sequence \mathcal{I} , we normalize it and transform it to a triplet of \mathbf{Q} , \mathbf{K} and \mathbf{V} , through linear layers. Then we employ the scaled dot-product attention mechanism to compute the attention values between the queries \mathbf{Q} and keys \mathbf{K} . Each output token is a weighted sum of all tokens using the attention values as weights, formulated as:

$$\text{Attention}(\mathbf{Q}, \mathbf{K}, \mathbf{V}) = \text{softmax}(\mathbf{Q}^\top \mathbf{K} / \sqrt{D}) \mathbf{V}, \quad (1)$$

where the token-to-token attention map $A = \text{softmax}(\mathbf{Q}^\top \mathbf{K} / \sqrt{D})$.

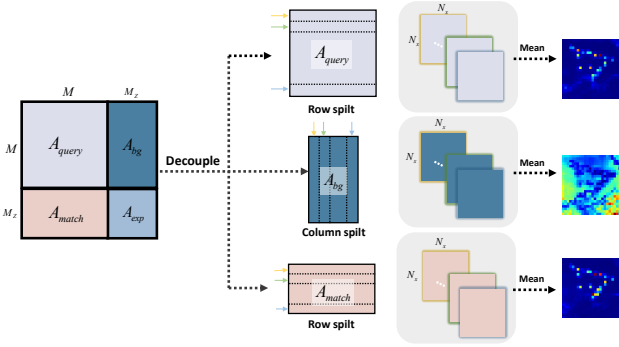


Figure 4: Decouple view for self-Attention in CACViT. Attention map in ViT can be split into four parts which can represent query image extraction, exemplars extraction, similarity matching, and background information. Here we show the attention map of the last layer in a decouple view.

In the presence of both query and exemplar tokens, we have $A \in \mathbb{R}^{(M+M_z) \times (M+M_z)}$, where M and M_z are the token number of the query image and the token number of exemplars, respectively. Note that, with the help of skip connection [7] in the self-attention block, the physical meanings of the query tokens and exemplar tokens are preserved through layers, which is a prerequisite of our approach and analysis.

By considering A directly, it is not intuitive to see how the self-attention mechanism can function as the feature extractor and matcher. Here we provide a fresh look at self-attention in CAC with a decoupled view.

First, we can split the token-to-token attention map A into 4 sub-attention maps as follow:

$$A = \begin{bmatrix} A_{query} & A_{bg} \\ A_{match} & A_{exp} \end{bmatrix}, \quad (2)$$

where $A_{query} \in \mathbb{R}^{M \times M}$, $A_{bg} \in \mathbb{R}^{M \times M_z}$, $A_{match} \in \mathbb{R}^{M_z \times M}$, and $A_{exp} \in \mathbb{R}^{M_z \times M_z}$.

As Figure 3 shows, A_{query} can be regarded as the self-attention map of the query image, which represents the most significant information within the image relevant to itself. A_{query} performs feature extraction for the query image identical to the ViT or the CNN backbone in previous work. Similarly, A_{exp} represents the self-attention map of the exemplars, which works as the feature extraction for the exemplars as in previous work.

A_{match} shown in Figure 3 can be regarded as cross-attention between the query image and exemplars, which thus can replace cross-attention layers used in previous ViT-based methods, taking the query image as the query and the exemplars as the key. In this way, A_{match} can perform the feature matching. In summary, compared with previous work, self-attention in CACViT executes feature extraction and matching in a simple and natural way.

In addition to the matching and extraction, we acquire an additional A_{bg} . As Figure 3 shows, the sum of every row of A_{query} is less than 1 because of A_{bg} . In this way, it is equivalent to introducing an additional weight to highlight the important regions, such as the objects of interest. At the same time, the background part

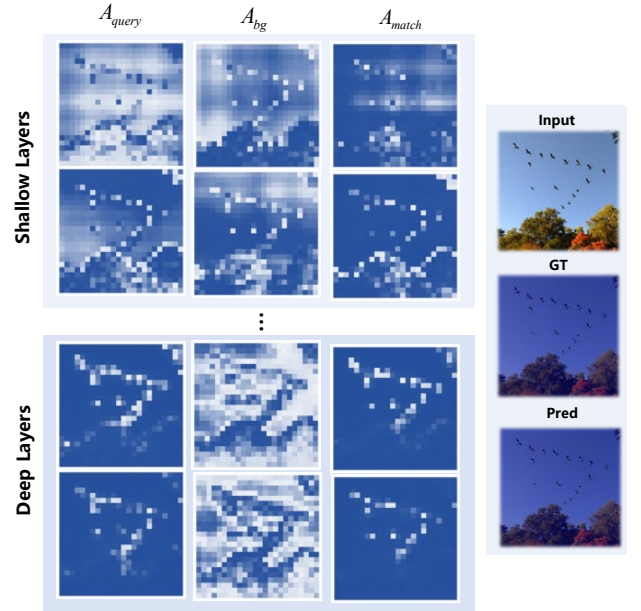


Figure 5: Visualizations of attention maps in a decoupled view for different layers. We visualize the attention map as Figure 4. (a) A_{query} and A_{match} highlight the foreground and suppress the background. (b) In the shallow layers, A_{bg} favors foreground; but in the deep layers, A_{bg} highlights background.

will be assigned with a small weight due to softmax normalization. We can use such information to further suppress background.

3.3 Analysis of Decoupled Attention Map

Visualization of Decoupled Attention. Figure 4 shows the procedure for how to visualize the attention maps. For the additional A_{bg} , we reshape every column to obtain the global attention map as Fig 4. Specifically, for every column $a_r \in \mathbb{R}^M$, we reshape it into $a_r \in \mathbb{R}^{N \times N}$, where N is the downsampled width and height for the query image. Then we compute the mean of every reshaped column used to indicate the response on the query image. We find that much attention is given to the background, which is neglected in the previous CAC model. A plausible explanation is that A_{bg} provides an extra attention token for restoring detailed information for feature extraction. With background information, CACViT can better resist the disturbance by background.

We also visualize the A_{query} and A_{match} in Fig 4. From Figure 4, we can find that the foreground part of the object to be counted receives strong attention weights. The visualization results and their functions are matched, which confirms the soundness of our interpretation above.

Yet, does the focus of the attention map change with the number of layers? We next visualize the attention maps with different depths of layers.

Visualization of Attention Maps in Different Layers. To explore how the attention of CACViT differs at different layers, we visualize the attention map for different layers in the same way

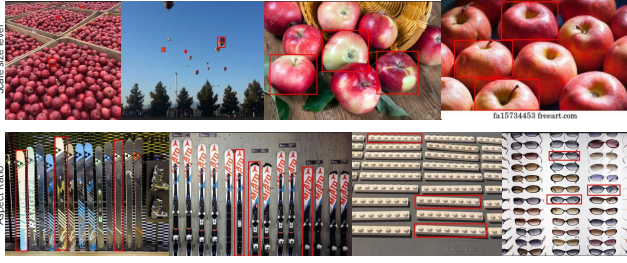


Figure 6: Examples of images with different scale levels and aspect ratio levels. The first and second rows display the variations in scale and in aspect ratio in the FSC147 dataset, respectively.

as above. From Fig. 5, we can see A_{query} and A_{match} attend to foreground consistently.

But for the A_{bg} , the attention of shallow and deep layers are different. At the shallow layer, A_{bg} tries to capture the foreground information. At the deep layer, A_{bg} tries to capture the background information. A plausible explanation for this phenomenon is that in the shallow layers, A_{bg} can provide distinct foreground information from exemplars for the query image, which assigns the foreground part more weight, and in the deep layer A_{bg} works to suppress the background noise.

With the help of additional A_{bg} , we can find the background noise in A_{query} is suppressed in deep layers so that we can infer more accurate counting results.

3.4 Scale and Magnitude Priors

While the self-attention mechanism in ViT is suitable for the CAC task, certain restrictions or functions within this structure can result in the loss of scale information, which plays an important role in the prediction of dense scenes. First, exemplars must be resized to fit the fixed-size tokens, which complicates the matching process. Second, the softmax function used to generate the attention map, which can represent the relative distribution of objects in the query image, can weaken the ability to express the number of targets in a query image.

In order to compensate for the loss and make our CACViT more suitable for the CAC task, we introduce aspect-ratio-aware scale embedding and order-of-magnitude embedding.

Aspect-Ratio-Aware Scale Embedding. To compensate for the loss of scale information, two key pieces of information need to be restored: the scale size level and the aspect ratio, which is shown in Figure 6. While scale-level information has been studied in previous work [25], aspect ratio information is often overlooked. Here we propose the scale embedding with further consideration of aspect ratio.

The embedding procedure is shown in Figure 7. Specifically, given an exemplar z_k , whose original width and height are W_k and H_k respectively. After resizing the function, we obtain a fixed size exemplar $z_k \in \mathbb{R}^{W_z \times H_z \times C}$, where W_z and H_z are the fixed-size height and width for every exemplar. First, to keep the width information of the exemplar, we generate a vector to represent width information by linear interpolation from 0 to the original

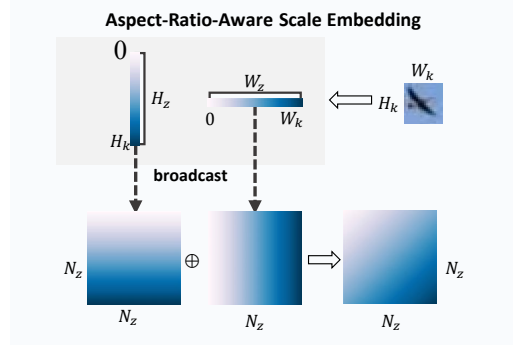


Figure 7: An illustration on how to compute the aspect-ratio-aware scale embedding for exemplar. For a exemplar with width W_k and height H_k , which will be resized to fixed width W_z and fixed height H_z .

width W_k . Then we can broadcast the vector to acquire a width map $\hat{W}_k \in \mathbb{R}^{W_z \times H_z}$. In the same way, we can obtain the height map $\hat{H}_k \in \mathbb{R}^{W_z \times H_z}$. Finally, we sum \hat{W}_k and \hat{H}_k as the scale embedding $S_k = \hat{W}_k + \hat{H}_k$. Then we can concatenate S_k with resized exemplar z_k to restore the scale information. Note that, in the way, we also encode the positional information for every patch by scale embedding.

Magnitude Embedding. In CACViT, we have the explicit similarity metric from the attention map. But the softmax function for relative distribution representation in the attention map will weaken the ability to express the number of objects in a query image. Therefore we present magnitude embedding to alleviate this phenomenon, which supplements the order-of-magnitude information for the query image from exemplars to compensate for the loss of normalization.

The order-of-magnitude information can be roughly represented by the ratio of the image size to the exemplar size. Specifically, we assume an exemplar is of width W_k and height H_k . Considering the patch size is of $W_p \times H_p$ pixels. The maximum capacity of a patch Mag_k conditioned on the exemplar z_k can be represented by:

$$Mag_k = \frac{W_p \times H_p}{W_k \times H_k}. \quad (3)$$

If we have K exemplars, we can compute the mean magnitude embedding from exemplars. Then we multiply the embedding with the similarity scores from the attention map to obtain the final similarity map.

4 EXPERIMENTS

4.1 Implementation Details

Network Structure: The network takes the image of size 384×384 as the input, which is first split into patches of size 16×16 , and then projected into 576 vectors. Each exemplar is of size 64×64 , then split into patches of size 16×16 , and projected into 16 vectors. Our feature extractor, pre-trained with MAE [6], consists of 12 transformer encoder blocks with a hidden dimension of 768, and each multi-head self-attention layer contains 12 heads. The following 3 extra transformer blocks with a hidden dimension of 512 are adopted to enhance the feature and reduce the dimension for upsampling. Our

Model	Backbone	Resolution	Two-stage training	Shots	Val MAE	Val RMSE	Test MAE	Test RMSE
FamNet+ [24]	ResNet50	384	×	1	26.55	77.01	26.76	110.95
BMNet+ [25]	ResNet50	[384,1584]	×	1	17.89	61.12	16.89	96.65
CounTR [16]	ViT-B & CNN	384	✓	1	13.15	49.72	12.06	90.01
CACViT (Ours)	ViT-B	384	×	1	11.41	41.04	8.62	29.92
FamNet+ [24]	ResNet-50	384	×	3	23.75	69.07	22.08	99.54
RCAC [5]	ResNet-50	384	×	3	20.54	60.78	20.21	81.86
BMNet+ [25]	ResNet-50	[384,1584]	×	3	15.74	58.53	14.62	91.83
SAFECount [31]	ResNet-18	512	×	3	15.28	47.20	14.32	85.54
SPDCN [15]	ResNet-18	576	×	3	14.59	49.97	13.51	96.80
CounTR [16]	ViT-B & CNN	384	✓	3	13.13	49.83	11.95	91.23
CACViT (Ours)	ViT-B	384	×	3	10.63	37.95	9.13	48.96

Table 1: Comparison with the state-of-the-art CAC approaches on the FSC-147 dataset. The upper part of the table presents the results on the 1-shot setting while the lower presents the 3-shots results. CounTR [16] need two-stage training regime [6]. Note that our 1-shot CACViT outperforms all of the previous methods even in the 3-shots setting.

regression decoder consists of 4 up-sampling layers with a hidden dimension of 256 as CounTR [16].

Training Details: To ensure a fair comparison, we use the same data augmentation as CounTR [16]. We apply AdamW [18] as the optimizer with a batch size of 8. The model is trained for 200 epochs with a learning rate of $1e-4$, a weight decay rate of 0.05, and 10 epochs to warm up. Our model is trained and tested on NVIDIA GeForce RTX 3090. Note that the CACViT consumes about 14GB of memory on a single GPU for 12 hours to train.

4.2 Datasets

The FSC147 Dataset. As the first large-scale dataset for class-agnostic counting, FSC147 [24] includes 6, 135 images from 147 categories varying from animals to vehicles. Besides, FSC147 has a wide range of object count from 7 to 3731, of which the average count is 56. Given one query image, three instances of the same category are randomly chosen as the exemplars by bounding boxes. To validate the generalization of the model, the categories in training, validation, and test set have no overlap.

4.3 Comparison with State of the Art

Quantitative Results. We compare our CACViT with CNN-based method FamNet+ [24], RCAC [5], BMNet+ [25], SAFECount [31], SPDCN [15], and the most recent state-of-the-art ViT-based method CounTR [16]. Note that some methods above do not report the performance under the 1-shot setting, so we do not compare with them in that setting.

As shown in Table 1, CACViT outperforms all the compared methods on both 1-shot and 3-shot settings significantly. In the 1-shot setting, CACViT achieves a relative improvement of 13.23% w.r.t validation MAE and 28.52% w.r.t test MAE compared with CounTR. Besides, CACViT reduces the validation RMSE by 17.45% and the test RMSE by 66.76%. Moreover, our method does not need self-supervised pre-train on the FSC147 dataset, which indicates

method	Model Size (M)	GFLOPs	#epochs
CounTR pretrain	112M	27G	300
CounTR finetune	99M	84G	1000*
CACViT (Ours)	99M	89G	200

Table 2: Comparison of the model size and FLOPs. * indicates that we obtain the #epochs on its official project page, which is not mentioned on paper.

the strong learning ability of the proposed framework. In a few-shot setting, compared with CounTR, CACViT generates a relative improvement of 19.04% w.r.t validation MAE and 23.60% w.r.t test MAE. One can also observe that CACViT reduces the validation RMSE by 23.84% and the test RMSE by 46.33% compared with CounTR, which validates the robustness of our method.

It is worth noting that CACViT on the 1-shot setting can even outperform all previous methods under the few-shot setting, which demonstrate that our CACViT can capture and match the features well even with just one exemplar.

Running Cost Evaluation. To verify whether our simplified structure can benefit the training, we compare our model size, floating point operations (FLOPs) with CounTR [16], which employs the same backbone as CACViT. The results are reported in Table 2. Note that CounTR does not report its epochs for finetune stage epochs in paper, we get the data from its official GitHub page. Our training setting is similar to CounTR [16]. However, 1) we exclude the self-supervised [6] pre-training on the FSC147 dataset compared with CounTR, which leads to a complex training strategy, and 2) we do not require an additional CNN to extract features of exemplars, which will cause varied feature spaces. One can easily observe that our CACViT can significantly reduce the training epochs from 1300 to 200 and simplify the training strategy into one stage while keeping the model size and FLOPs comparable to that of CounTR.

No.	BG	SE	ME	Val MAE	Val RMSE
B1				13.00	48.37
B2	✓			12.40	48.62
B3	✓	✓		10.61	40.42
B4	✓		✓	12.32	42.42
B5	✓	✓	✓	10.62	37.95

No.	BG	SE	ME	Test MAE	Test RMSE
B6				13.67	117.60
B7	✓			11.56	90.41
B8	✓	✓		10.89	78.03
B9	✓		✓	11.61	83.06
B10	✓	✓	✓	9.13	48.96

Table 3: Ablation study on the FSC147 dataset. BG denotes the background suppression component A_{bg} in self-attention, SE refers to scale embedding, and ME denotes magnitude embedding.

Qualitative Analysis. For qualitative analysis, we compare our CACViT with the state-of-the-art CNN-based model BMNet+ [25] and the most recent state-of-the-art ViT-based model CounTR [16]. As shown in Fig 8, CACViT outperforms other methods in different scenes, including images with multiple classes, or in dense environments and colorful environments. For hard cases involving interference from other classes (the 1st and 2nd column), our method allows better learning of the characteristics of the objects to be counted. From the 1st column in Fig 8, other methods confuse blueberries for strawberries, resulting in over-prediction compared with ground truth. For the dense environment (the 3rd, 4th, 5th, 7th, 8th, 9th, and 10th columns), we can still get accurate density maps. For inputs with different colors within the class (from the 6th column to the 9th column), our method can capture the key features therefore enhance the generalization ability. For the 7th column in Fig 8, a dense and colorful environment, BMNet+ overestimates the counting result because of the dense environment, CounTR underestimates the counting result affected by the color, while our CACViT keeps a consistent accuracy.

4.4 Ablation Study

We perform the ablation study on FSC147 and provide quantitative results in Table 3. The plain version of CACViT is employed as the baseline which only consists of standard feature extraction and matching blocks by self-attention, and the A_{bg} part in attention map are masked (B1 and B6).

Background suppression by A_{bg} . By comparing B6 and B7 in Table 3, one can observe that background suppression can introduce a relative improvement of 15.44% w.r.t. MAE and 23.12% w.r.t. RMSE on the test set. The performance boost indicates that A_{bg} part in the attention map can help to suppress the background noise for CACViT.

Aspect-ratio-aware scale embedding. As shown in Table 3, the aspect-ratio-aware scale embedding brings a relative improvement of 14.44% MAE and 16.87% RMSE on the validation set and

Method	Val MAE	Val RMSE	Test MAE	Test RMSE
BMN-SE [25]	11.65	43.50	11.57	92.47
Sin [27]	11.02	42.86	9.86	56.88
$\text{lin}(h) \oplus \text{lin}(w)$ (ours)	11.32	42.89	10.87	57.18
$\text{lin}(h) + \text{lin}(w)$ (ours)	10.63	37.95	9.13	48.96

Table 4: Ablation study on methods for scale embedding. BMN-SE [25] represents the scale embedding method from BMNet+, which adds width and height up to restore scale information. Sin [27] denotes the position embedding method from Transformer, which adds position information for input. lin denotes the linspace which can obtain vector for height and width, and \oplus represents channel-wise concatenation.

n	Val MAE	Val RMSE	Test MAE	Test RMSE
3	16.67	58.57	16.52	107.41
6	13.17	43.11	12.69	70.20
9	12.77	44.46	11.83	66.45
12	10.63	37.95	9.13	48.96

Table 5: Ablation study on the number of attention layers in the ViT encoder.

5.80% MAE and 13.69% RMSE on the test set (cf. B2 vs. B3 and B7 vs. B8), which verifies that the aspect-ratio-aware scale embedding can restore original size information for exemplars, and therefore matters in CAC task. Note that, the performance on RMSE further demonstrates that the SE module can boost the robustness of the model.

Methods for scale embedding. Then we investigate the impact of the methods for scale embedding. Here we compare our SE method with the previous scale embedding method from BMNet+ [25], which divides the scale space into 20 levels. Besides, to validate the capability of our method for location encoding, we compare our method with the position embedding in Transformer [27]. The results are shown in Table 4. Compared with the previous scale embedding method in BMNet+, our method perform better by providing extra aspect ratio information and position embedding (the 1st and 4th row). From the result in row 2, one can see that position embedding is important for CACViT. Compared with pure positional embedding, our method can provide better scale information. Then we try to discuss possible ways to integrate the width information and height information (the 3rd row and 4th row), the results show that adding the height map and width map outperforms concatenating them in channel dimension.

Magnitude Embedding. The comparison of B2 vs. B4 and B7 vs. B9 demonstrates that magnitude embedding improves the validation RMSE by 6.2 and test RMSE by 7.35. However, the performance boost on MAE is marginal or even declines slightly. The reason may lie in that resized exemplars provide a wrong prior of object size which confuses the model.



Figure 8: Qualitative results on the FSC147 dataset. Different challenges are shown in the selected inputs, including images with multiple classes, dense environments, and colorful environments. Our method consistently outperforms previous methods with more precise locations.

Cooperation between Scale Embedding and Magnitude Embedding. By Comparing B8 with B10 in Table 3, one can observe that magnitude embedding can lead to a relative improvement of 21.36% w.r.t. MAE and 41.05% w.r.t. RMSE on the test set. Note that the improvement is much more significant compared with the situation without scale embedding, which indicates that the combination of scale embedding and magnitude embedding can further boost the performance. The synergy between the scale embedding and magnitude embedding can provide scale prior for input and output separately, therefore CACViT can capture the scale prior all the time.

The number of attention layers. Here we investigate whether the number n of layers in the ViT encoder can affect the extraction and matching. Since the ViT pre-trained with MAE [6] contains 12 layers attention layers, we experiment with $n = 3, 6, 9, 12$ and report their results in Table 5. Note that our CACViT outperforms the state-of-the-art method CounTR [16] with only 9 layers of ViT encoder, which verifies the better use of self-attention mechanism.

4.5 Cross-Dataset Generalization.

We test the generality of the model on a car counting dataset CARPK[9]. CARPK contains 1, 448 images of parking lots in a bird view, which differs significantly from the images in FSC147. We exclude the “cars” category within FSC147 to ensure that training and test categories have no overlap.

Results are reported in Table 6. We first focus on models without fine-tuning on the CARPK dataset. One can observe that our model exhibits strong generality. Compared with BMNet+[25], CACViT

Method	Fine-tuned	MAE	RMSE
FamNet+	×	28.84	44.47
RCAC	×	17.98	24.21
SAFECount	×	16.66	24.08
BMNet+	×	10.44	13.77
CounTR	×	-	-
CACViT (Ours)	×	8.30	11.18
FamNet+	✓	18.19	33.66
RCAC	✓	13.62	19.08
SAFECount	✓	5.33	7.04
BMNet+	✓	5.76	7.83
CounTR	✓	5.75	7.45
CACViT (Ours)	✓	4.91	6.49

Table 6: Generalization performance on the CARPK dataset. All models are pre-trained on the FSC147 dataset without the ‘cars’ class. “fine-tuned” denotes whether the pre-trained models are further fine-tuned on the CARPK dataset.

generates a relative performance gain of 20.50% MAE. Moreover, CACViT still retains advantages when compared with CounTR in the fine-tuning scenario, which demonstrates that our designs are orthogonal to fine-tuning.

5 CONCLUSIONS

In this work, we propose a simple yet efficient ViT-based model CACViT for CAC. Specifically, from a decoupled view of the attention mechanism, we show that the ViT is naturally suitable for the CAC task. And we propose an extract-and-match paradigm for CAC based on the ViT architecture. Then we introduce aspect-ratio-aware scale embedding and magnitude embedding to compensate for the scale loss in ViT. Our CACViT achieves state-of-the-art performance on the large-scale dataset FSC147, and we also verify the generality on the car counting dataset CARPK.

Our current framework still suffers from large number of parameters and computation workload. We consider to reduce the computational costs by designing better feature representations based on our simple model in the future work. Moreover, we will extend our work of few-shot class-agnostic counting to zero-shot class-agnostic counting.

REFERENCES

- [1] Shahira Aousamra, Minh Hoai, Dimitris Samaras, and Chao Chen. 2021. Localization in the crowd with topological constraints. In *Proceedings of the AAAI Conference on Artificial Intelligence*, Vol. 35. 872–881.
- [2] Xinkun Cao, Zhipeng Wang, Yanyun Zhao, and Fei Su. 2018. Scale aggregation network for accurate and efficient crowd counting. In *Proceedings of the European conference on computer vision (ECCV)*. 734–750.
- [3] Zhi-Qi Cheng, Qi Dai, Hong Li, Jingkuan Song, Xiao Wu, and Alexander G Hauptmann. 2022. Rethinking spatial invariance of convolutional networks for object counting. In *Proceedings of the IEEE/CVF Conference on Computer Vision and Pattern Recognition*. 19638–19648.
- [4] Alexey Dosovitskiy, Lucas Beyer, Alexander Kolesnikov, Dirk Weissenborn, Xiuhua Zhai, Thomas Unterthiner, Mostafa Dehghani, Matthias Minderer, Georg Heigold, Sylvain Gelly, et al. 2020. An image is worth 16x16 words: Transformers for image recognition at scale. *arXiv preprint arXiv:2010.11929* (2020).
- [5] Shenjian Gong, Shanshan Zhang, Jian Yang, Dengxin Dai, and Bernt Schiele. 2022. Class-Agnostic Object Counting Robust to Intra-class Diversity. In *Computer Vision—ECCV 2022: 17th European Conference, Tel Aviv, Israel, October 23–27, 2022, Proceedings, Part XXXIII*. Springer, 388–403.
- [6] Kaiming He, Xinlei Chen, Saining Xie, Yanghao Li, Piotr Dollár, and Ross Girshick. 2022. Masked autoencoders are scalable vision learners. In *Proceedings of the IEEE/CVF Conference on Computer Vision and Pattern Recognition*. 16000–16009.
- [7] Kaiming He, Xiangyu Zhang, Shaoqing Ren, and Jian Sun. 2016. Deep residual learning for image recognition. In *Proceedings of the IEEE conference on computer vision and pattern recognition*. 770–778.
- [8] Yuhang He, Zhiheng Ma, Xing Wei, Xiaopeng Hong, Wei Ke, and Yihong Gong. 2021. Error-aware density isomorphism reconstruction for unsupervised cross-domain crowd counting. In *Proceedings of the AAAI conference on artificial intelligence*, Vol. 35. 1540–1548.
- [9] Meng-Ru Hsieh, Yen-Liang Lin, and Winston H Hsu. 2017. Drone-based object counting by spatially regularized regional proposal network. In *Proceedings of the IEEE international conference on computer vision*. 4145–4153.
- [10] Haroon Idrees, Muhammad Tayyab, Kishan Athrey, Dong Zhang, Somaya Al-Maadeed, Nasir Rajpoot, and Mubarak Shah. 2018. Composition loss for counting, density map estimation and localization in dense crowds. In *Proceedings of the European conference on computer vision (ECCV)*. 532–546.
- [11] Issam H Laradji, Negar Rostamzadeh, Pedro O Pinheiro, David Vazquez, and Mark Schmidt. 2018. Where are the blobs: Counting by localization with point supervision. In *Proceedings of the European conference on computer vision (ECCV)*. 547–562.
- [12] Dingkan Liang, Xiwu Chen, Wei Xu, Yu Zhou, and Xiang Bai. 2022. Transcrowd: weakly-supervised crowd counting with transformers. *Science China Information Sciences* 65, 6 (2022), 160104.
- [13] Dingkan Liang, Wei Xu, and Xiang Bai. 2022. An end-to-end transformer model for crowd localization. In *Computer Vision—ECCV 2022: 17th European Conference, Tel Aviv, Israel, October 23–27, 2022, Proceedings, Part I*. Springer, 38–54.
- [14] Hui Lin, Zhiheng Ma, Rongrong Ji, Yaowei Wang, and Xiaopeng Hong. 2022. Boosting crowd counting via multifaceted attention. In *Proceedings of the IEEE/CVF Conference on Computer Vision and Pattern Recognition*. 19628–19637.
- [15] Wei Lin, Kunlin Yang, Xinzhu Ma, Junyu Gao, Lingbo Liu, Shinan Liu, Jun Hou, Shuai Yi, and Antoni B Chan. 2022. Scale-Prior Deformable Convolution for Exemplar-Guided Class-Agnostic Counting. (2022).
- [16] Chang Liu, Yujie Zhong, Andrew Zisserman, and Weidi Xie. 2022. Count: Transformer-based generalised visual counting. *arXiv preprint arXiv:2208.13721* (2022).
- [17] Lingbo Liu, Jiaqi Chen, Hefeng Wu, Tianshui Chen, Guanbin Li, and Liang Lin. 2020. Efficient crowd counting via structured knowledge transfer. In *Proceedings of the 28th ACM international conference on multimedia*. 2645–2654.
- [18] Ilya Loshchilov and Frank Hutter. 2017. Decoupled weight decay regularization. *arXiv preprint arXiv:1711.05101* (2017).
- [19] Erika Lu, Weidi Xie, and Andrew Zisserman. 2019. Class-agnostic counting. In *Computer Vision—ACCV 2018: 14th Asian Conference on Computer Vision, Perth, Australia, December 2–6, 2018, Revised Selected Papers, Part III 14*. Springer, 669–684.
- [20] Hao Lu, Zhiguo Cao, Yang Xiao, Bohan Zhuang, and Chunhua Shen. 2017. TasselNet: counting maize tassels in the wild via local counts regression network. *Plant methods* 13, 1 (2017), 1–17.
- [21] Zhiheng Ma, Xing Wei, Xiaopeng Hong, and Yihong Gong. 2020. Learning scales from points: A scale-aware probabilistic model for crowd counting. In *Proceedings of the 28th ACM International Conference on Multimedia*. 220–228.
- [22] Simon Madec, Xiuliang Jin, Hao Lu, Benoit De Solan, Shouyang Liu, Florent Duyme, Emmanuelle Heritier, and Frederic Baret. 2019. Ear density estimation from high resolution RGB imagery using deep learning technique. *Agricultural and forest meteorology* 264 (2019), 225–234.
- [23] Daniel Onoro-Rubio and Roberto J López-Sastre. 2016. Towards perspective-free object counting with deep learning. In *Computer Vision—ECCV 2016: 14th European Conference, Amsterdam, The Netherlands, October 11–14, 2016, Proceedings, Part VII 14*. Springer, 615–629.
- [24] Viresh Ranjan, Udbhav Sharma, Thu Nguyen, and Minh Hoai. 2021. Learning to count everything. In *Proceedings of the IEEE/CVF Conference on Computer Vision and Pattern Recognition*. 3394–3403.
- [25] Min Shi, Hao Lu, Chen Feng, Chengxin Liu, and Zhiguo Cao. 2022. Represent, compare, and learn: A similarity-aware framework for class-agnostic counting. In *Proceedings of the IEEE/CVF Conference on Computer Vision and Pattern Recognition*. 9529–9538.
- [26] Weibo Shu, Jia Wan, Kay Chen Tan, Sam Kwong, and Antoni B Chan. 2022. Crowd counting in the frequency domain. In *Proceedings of the IEEE/CVF Conference on Computer Vision and Pattern Recognition*. 19618–19627.
- [27] Ashish Vaswani, Noam Shazeer, Niki Parmar, Jakob Uszkoreit, Llion Jones, Aidan N Gomez, Łukasz Kaiser, and Illia Polosukhin. 2017. Attention is all you need. *Advances in neural information processing systems* 30 (2017).
- [28] Qi Wang, Junyu Gao, Wei Lin, and Xuelong Li. 2020. NWPU-crowd: A large-scale benchmark for crowd counting and localization. *IEEE transactions on pattern analysis and machine intelligence* 43, 6 (2020), 2141–2149.
- [29] Qiangqiang Wu, Jia Wan, and Antoni B Chan. 2021. Dynamic momentum adaptation for zero-shot cross-domain crowd counting. In *Proceedings of the 29th ACM International Conference on Multimedia*. 658–666.
- [30] Shuo-Diao Yang, Hung-Ting Su, Winston H Hsu, and Wen-Chin Chen. 2021. Class-agnostic few-shot object counting. In *Proceedings of the IEEE/CVF Winter Conference on Applications of Computer Vision*. 870–878.
- [31] Zhiyuan You, Kai Yang, Wenhan Luo, Xin Lu, Lei Cui, and Xinyi Le. 2023. Few-shot object counting with similarity-aware feature enhancement. In *Proceedings of the IEEE/CVF Winter Conference on Applications of Computer Vision*. 6315–6324.
- [32] Cong Zhang, Hongsheng Li, Xiaogang Wang, and Xiaokang Yang. 2015. Cross-scene crowd counting via deep convolutional neural networks. In *Proceedings of the IEEE conference on computer vision and pattern recognition*. 833–841.
- [33] Zhikang Zou, Xiaoye Qu, Pan Zhou, Shuangjie Xu, Xiaoqing Ye, Wenhao Wu, and Jin Ye. 2021. Coarse to fine: Domain adaptive crowd counting via adversarial scoring network. In *Proceedings of the 29th ACM International Conference on Multimedia*. 2185–2194.